

Slipstream Modeling and Control Allocation of a Distributed Heterogeneous Electric Propulsion Tandem-Wing UAV

Yuhang Xie[1,2], Zhou Zhou[1,2]

[1] School of Aeronautics, Northwestern Polytechnical University, Xi'an 710072, China

[2] National Key Laboratory of Aircraft Configuration Design, Xi'an 710072, China

Abstract

Distributed heterogeneous electric propulsion tandem-wing UAVs adopting a fixed-point high-pitch-angle takeoff mode combine superior takeoff and landing capability with high aerodynamic efficiency. However, the aerodynamic–propulsive coupling induced by propeller slipstreams, together with the coupled over-actuated characteristics of aerodynamic control surfaces and multiple propulsion units, poses significant challenges to modeling and control allocation. In this paper, a propeller slipstream model considering finite-scale effects is established and validated through ground static experiments. Based on this model, a control allocation strategy is designed for the coupled over-actuated system, and full-process simulations from fixed-point high-pitch takeoff to steady climb are conducted. The results show that the proposed slipstream model achieves good accuracy, and that the control allocation strategy can significantly suppress pitch attitude oscillations during the high-angle-of-attack takeoff phase while requiring relatively small control inputs.

Keywords: distributed electric propulsion, high-pitch takeoff, propeller slipstream model, control allocation

1. Introduction

With the rapid development of electric motors, batteries, and power electronics[1], distributed electric propulsion (DEP) has become an important direction in the design of vertical/short takeoff and landing (VTOL/STOL) unmanned aerial vehicles (UAVs)[2], [3]. Compared with conventional propulsion architectures based on a single high-thrust unit, DEP distributes multiple small propulsion units around the wing or airframe. This arrangement not only improves the flexibility of propulsion-system integration, but also exploits the aerodynamic–propulsive coupling between propeller slipstreams and the wing. In low-speed and high-angle-of-attack conditions, this coupling can increase the local dynamic pressure over the wing, thereby improving takeoff and landing performance as well as low-speed control authority [3]. In addition, the independent regulation of multiple propulsion units provides the aircraft with greater control degrees of freedom and redundancy, enabling differential thrust to participate in attitude control and thus enhancing control authority during complex flight phases [4], [5].

For tandem-wing UAVs adopting a fixed-point high-pitch-angle takeoff mode, DEP technology has particularly important application value. On the one hand, the slipstreams generated by distributed propellers can provide additional dynamic pressure over the wing and control surfaces under low-speed or even near-zero freestream conditions, thereby improving lift generation and control moment capability during the initial takeoff phase. On the other hand, the combined layout of the front and rear wings with multiple propulsion units enables attitude control through the coordinated use of aerodynamic control surfaces and differential thrust.

However, this configuration also introduces more complex modeling and control challenges. Propeller slipstreams modify the local flow velocity and effective angle of attack over the wing and control-surface regions, causing the aerodynamic forces and control effectiveness to vary significantly with thrust, airspeed, and angle of attack. Meanwhile, the aerodynamic control surfaces and multiple propulsion units exhibit pronounced redundancy and coupling, which further complicates the control allocation problem. Therefore, accurately describing the effects of propeller slipstreams on aerodynamic forces and control-surface effectiveness, and designing an

appropriate control allocation strategy on this basis, are key issues that must be addressed for fixed-point high-pitch takeoff control of DEP tandem-wing UAVs.

To address the modeling of propeller slipstream effects associated with aerodynamic–propulsive coupling, Ting et al.[6] proposed an interference model based on matched asymptotic expansions. Nederlof[7] investigated an image vortex correction method based on potential flow theory to address lift overestimation. However, due to the complexity of solving rotational flow equations and the intricate mathematical formulations involved, both approaches incur high computational costs, rendering them impractical for efficient flight dynamics modeling. Qin et al.[8] proposed a modeling approach based on momentum theory and experimental corrections, but the neglect of finite slipstream dimension effects led to discrepancies between theoretical predictions and experimental data. Patterson et al.[9] proposed a simplified method based on thin-wing theory and a point vortex model, employing a correction factor to account for finite slipstream height. However, this factor explicitly includes the freestream velocity as a denominator, resulting in a mathematical singularity under zero-freestream conditions.

For the over-actuated control allocation problem of DEP aircraft, Qin et al. [10] proposed an iterative control allocation method based on coordinate transformation for DEP vertical takeoff and landing aircraft. By decomposing the nonlinear control effectiveness model into two subsystems and solving them iteratively, this method improves the applicability of control allocation across different flight modes. Wang et al.[11] investigated heterogeneous redundant control mechanisms in distributed propulsion configurations and adopted a weighted pseudo-inverse method to coordinate the control relationship between aerodynamic control surfaces and propulsive actuators. Suiçmez et al.[12] integrated an optimization-based control allocation method into an incremental nonlinear dynamic inversion controller to address actuator saturation and multi-channel coupling in eVTOL aircraft controlled purely by thrust vectoring. de Heer et al.[13] proposed an incremental nonlinear control allocation method for aircraft with distributed electric propulsion, in which aerodynamic control surfaces and propulsion units are jointly included in the allocation process, with propeller power minimization as the optimization objective. Yılmaz and German[14] developed a nonlinear control allocation optimization method for an over-actuated tandem tiltwing eVTOL aircraft, accounting for aerodynamic–propulsive coupling and aerodynamic interference among components. Their results showed that nonlinear mappings considering aerodynamic interactions can improve the accuracy of force and moment command tracking.

In view of the above issues, the main contributions of this paper are summarized as follows:

- An aerodynamic–propulsive coupling model considering the finite-scale correction of propeller slipstreams is established, and its accuracy is validated through ground-based propeller slipstream experiments.
- Based on the heterogeneous inboard–outboard propulsion system and the coupled control characteristics of aerodynamic control surfaces under propeller slipstream effects, the attainable control moment sets of differential thrust and aerodynamic control surfaces are calculated and analyzed.
- A control allocation strategy is developed according to the calculated attainable moment sets. Full-process simulations from fixed-point high-pitch takeoff to steady climb are conducted to verify the effectiveness of the proposed control allocation strategy.

2. Modeling

2.1 Configuration Characteristics

The basic configuration of the Distributed Heterogeneous Electric Propulsion (DHEP) tandem-wing UAV is illustrated in Figure 1. The UAV has a total mass of 3 kg. Both the front and rear wings have a span of 1.2 m, with a Mean Aerodynamic Chord (MAC) of 0.3 m. The design cruise speed is 11 m/s. This UAV employs a fixed-point high-pitch-angle takeoff mode. Specifically, the four inboard propulsion units are responsible for providing high thrust during the low-speed takeoff phase, while the four outboard propulsion units are optimized for cruise propulsion. The arrangement of the heterogeneous propulsion units is shown in Figure 2.

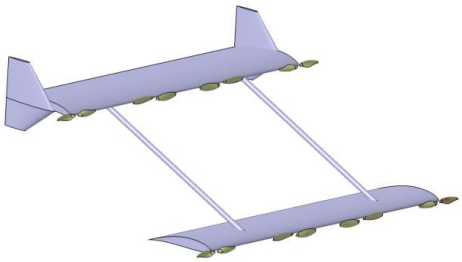


Figure 1 – 3D model of DHEP-UAV.

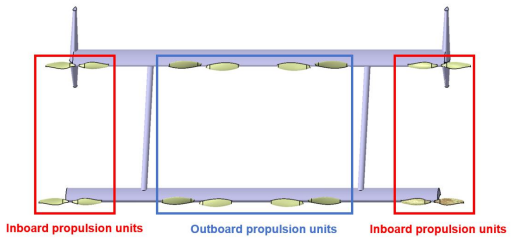


Figure 2 – Heterogeneous propulsion units.

2.2 Distributed Heterogeneous Electric Propulsion Model

The distributed propulsion UAV investigated in this paper features a heterogeneous propeller design for the inboard and outboard sections, although the propulsion units in both sections are equipped with identical motors. Motor performance data were obtained through ground static experiments. Curve fitting techniques were employed to model the relationships between the propulsion system's throttle and total power, as well as throttle and motor efficiency as shown in Figure 3.

The inboard propulsion units utilize APC 9x4.7 inch propellers, while the outboard units utilize APC 8x6 inch propellers. The aerodynamic performance parameters for the propellers were derived from official APC technical data sheets and validated via ground static experiments, which demonstrated good agreement. Subsequently, curve fitting techniques were used to model the relationships between advance ratio and thrust coefficient, and advance ratio and efficiency for both the inboard and outboard propellers as shown in Figure 4.

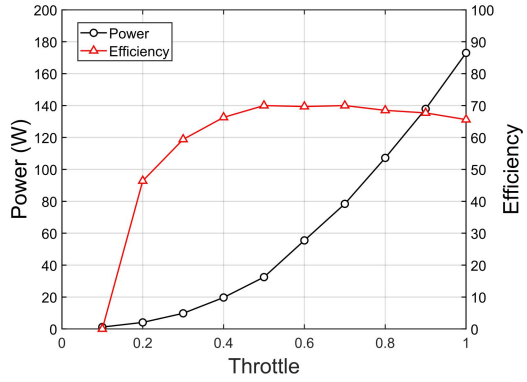


Figure 3 – Variation of motor power and efficiency with throttle.

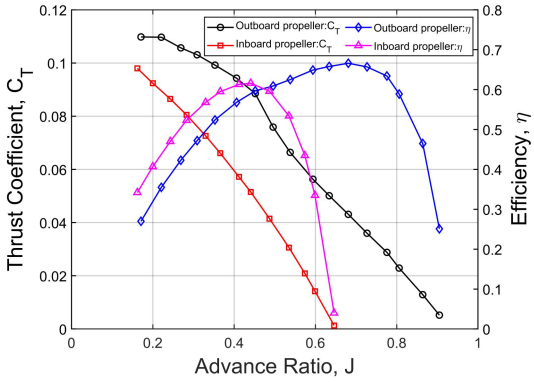


Figure 4 – Variation of thrust coefficient and efficiency with advance ratio.

2.3 Slipstream Enhanced Aerodynamic Model

By modeling the propeller slipstream velocity based on momentum theory[15], the propeller induced velocity is given by:

$$v_0 = \frac{1}{2}\left(-V_\infty + \sqrt{V_\infty^2 + \frac{8C_T n^2 D^2}{\pi}}\right) \tag{1}$$

As the propeller slipstream propagates downstream, its velocity continues to increase, and the slipstream diameter gradually contracts. In this paper, the slipstream velocity at the wing leading edge is adopted as the average induced velocity of an individual slipstream unit:

$$v_0(x) = v_0\left[1 + \frac{x/R_p}{\sqrt{1+(x/R_p)^2}}\right] \tag{2}$$

Given the finite height of the propeller slipstream, equating it to an infinite freestream leads to an overestimation of lift enhancement; thus, a finite height correction factor is introduced. Literature indicates that lift enhancement is governed by scale and velocity: it diminishes as the slipstream height-to-chord ratio decreases or as the disparity between slipstream and freestream velocities increases.

According to Ting et al.[6], $K_L$is defined as the ratio of lift under the influence of slipstream to the lift without slipstream. Curve fitting techniques were employed to model the relationship of K_L with respect to the ratio of slipstream height to wing chord h/c, and the ratio of the square of slipstream velocity to the square of freestream velocity V_J/V_∞. The fitting results are shown in Figure 5.

$$K_L = 0.109\left(\frac{h}{c}\right)^3 - 0.233\left(\frac{h}{c}\right)^2\left(\frac{V_J}{V_\infty}\right)^2 - 0.26\left(\frac{h}{c}\right)^2 + 1.01\left(\frac{h}{c}\right)\left(\frac{V_J}{V_\infty}\right)^2 - 0.444\left(\frac{h}{c}\right) - 0.019\left(\frac{V_J}{V_\infty}\right)^2 + 0.925 \tag{3}$$

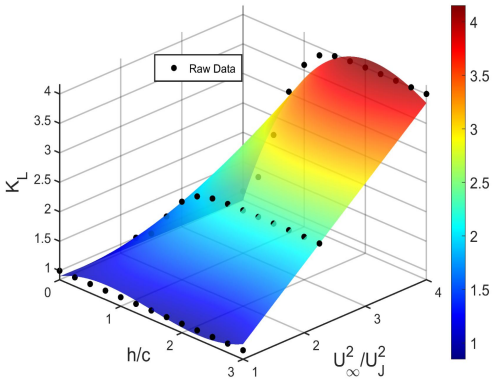


Figure 5 – Fitted curve of the lift ratio.

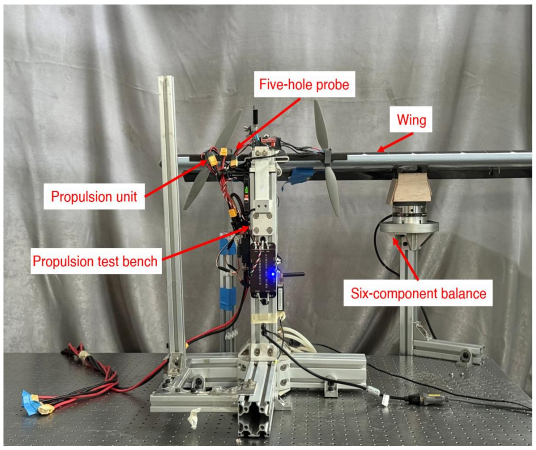


Figure 6 –Slipstream experimental test platform.

From K_L, the slipstream finite height correction factor β can be calculated:

$$\beta = \frac{K_{C_L} V_\infty^2}{V_J^2} \tag{4}$$

When the freestream velocity is 0, the ratio of slipstream velocity to freestream velocity, V_J/V_∞, tends towards infinity, causing the finite height correction factor β to become invalid under zero freestream conditions. To ensure the generality of the model, a limiting mechanism is introduced for V_J/V_∞, and the upper limit of the velocity ratio is defined as $K = 2$. The expression for the velocity ratio after limiting is:

$$\gamma_{\lim} = \begin{cases} K, & \frac{V_J}{V_\infty} > K \\ \frac{V_J}{V_\infty}, & \frac{V_J}{V_\infty} \le K \end{cases} \tag{5}$$

The propeller slipstream not only increases the dynamic pressure over the wing surface, but also changes the local angle of attack within the slipstream-affected region. The local angle of attack in the propeller slipstream can be calculated as

$$\alpha_{slip} = \frac{V_\infty \sin(\alpha)}{V_\infty \cos(\alpha) + v_0(x_{le})} \tag{6}$$

where α denotes the angle of attack of the wing in the freestream. For a distributed-propulsion UAV, lift augmentation is achieved by increasing the dynamic pressure over the wing surface through propeller slipstreams and by modifying the local angle of attack. Therefore, the slipstream velocity and local angle of attack obtained from the above equations are used to calculate the lift, drag, and pitching moment in the slipstream-affected region. In addition, the correction factor β is introduced to account for the finite-height effect of the propeller slipstream. The corresponding expressions are given by

$$\begin{cases} L_{slip} = 0.5\rho V_{slip}^2 S_{slip} C_L(\alpha_{slip})\beta \\ D_{slip} = 0.5\rho V_{slip}^2 S_{slip} C_D(\alpha_{slip})\beta \\ M_{slip} = 0.5\rho V_{slip}^2 S_{slip} C_M(\alpha_{slip})\beta \end{cases} \tag{7}$$

In the remaining regions, the aerodynamic forces and pitching moment are generated by the freestream. They are calculated as

$$\begin{cases} L_{free} = 0.5\rho V_{\infty}^2 S_{free} C_L(\alpha) \\ D_{free} = 0.5\rho V_{\infty}^2 S_{free} C_D(\alpha) \\ M_{free} = 0.5\rho V_{\infty}^2 S_{free} C_M(\alpha) \end{cases} \tag{8}$$

The aerodynamic coefficients in the freestream are obtained from CFD simulations. The total aerodynamic forces and pitching moment of the aircraft are obtained by superimposing the aerodynamic forces and moment in the slipstream-affected region and those in the freestream region:

$$\begin{cases} L_{total} = L_{slip} + L_{free} \\ D_{total} = D_{slip} + D_{free} \\ M_{total} = M_{slip} + M_{free} \end{cases} \tag{9}$$

2.4 Experimental Validation of the Slipstream Model

To validate the model established in this section, ground tests of the propeller slipstream were conducted. The slipstream experimental test platform is shown in Figure 6. Figures 7 and 8 show the experimental platforms for slipstream-induced lift measurement and slipstream velocity measurement, respectively. The wing lift and slipstream velocity were measured under different throttle settings. Since the freestream velocity was zero in the ground tests, the wing lift was generated entirely by the induced velocity of the propeller slipstream. Therefore, the model developed in this section was used to calculate the wing lift under this condition, and the results were compared with the experimental measurements for validation.

The tests included two cases: lift augmentation induced by a single propeller and lift augmentation induced by two counter-rotating propellers. Under different throttle commands, the propellers were driven by the motors to generate slipstreams, and the wing located downstream of the propellers consequently produced lift. The wing was rigidly connected to a six-component balance mounted on the test platform. The balance measured the forces and moments along three axes, from which the wing lift under different throttle settings was obtained. The rotational speed of the propeller–motor system and the power of the propulsion system were measured using an optical tachometer and a propulsion test bench, respectively, and the data were recorded by a data acquisition system. In addition, a supplementary slipstream velocity measurement test was conducted. To eliminate the influence of the wing on the measured slipstream velocity, this test was performed after removing the wing. The slipstream velocity was measured using a five-hole probe.

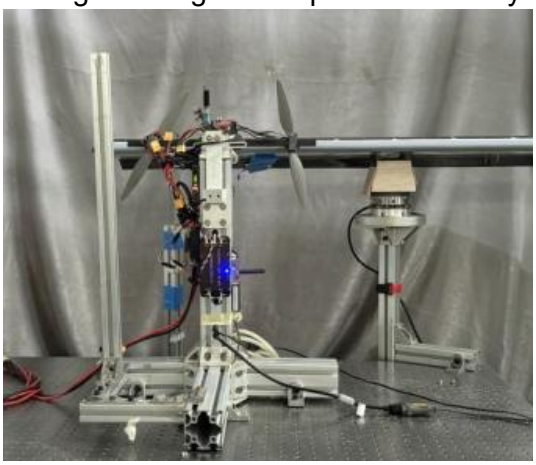


Figure 7 – Slipstream-induced lift test platform.

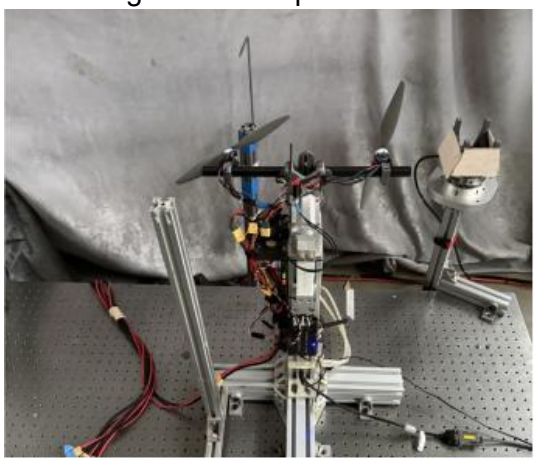


Figure 8 –Slipstream velocity measurement platform.

The data acquired by the balance were filtered to reduce the influence of experimental noise. To validate the accuracy of the aerodynamic model proposed in this paper, the slipstream parameters predicted by the model were compared with the ground-test measurements. The comparison results are shown in Figures 9 and 10.

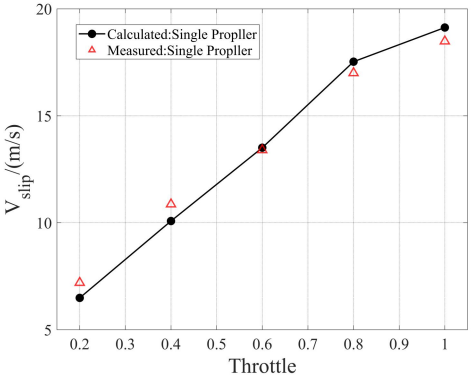


Figure 9 – Comparison of experimental and calculated slipstream velocity.

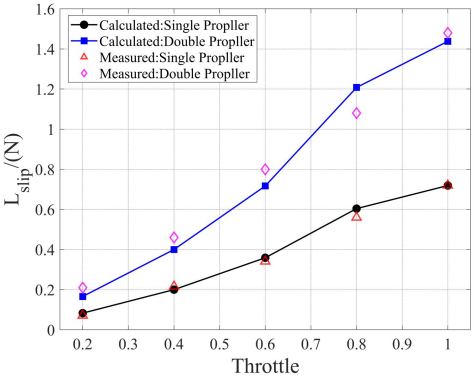


Figure 10 – Comparison of experimental and calculated slipstream lift.

Comparison with the slipstream test results shows that the lift and slipstream velocity predicted by the proposed model agree well with the experimental measurements. In the slipstream velocity measurement test, the distance between the probe and the propeller plane was greater than the propeller diameter. The results indicate that the induced velocity of the propeller slipstream undergoes a distinct contraction and acceleration process downstream of the propeller plane. In the slipstream-induced lift test, under the same throttle setting, the lift induced by the slipstream of two counter-rotating propellers was approximately twice that induced by a single propeller. This indicates that the slipstream interaction between different propulsion units of the distributed-propulsion UAV is relatively weak and can be approximated as a linear superposition of multiple single-propeller effects.

3. Attainable Moment Set Calculation and Control Allocation Design for Redundant Coupled Effectors

3.1 Analysis of Redundant Coupled Effector Characteristics under Propeller Slipstream Effects

Based on the propeller slipstream model, the control capability of the distributed heterogeneous electric propulsion tandem-wing UAV is further analyzed. This configuration employs two types of control effectors: aerodynamic control surfaces and multiple heterogeneous propulsion units. The propulsion system can directly generate pitching and yawing moments through longitudinal or lateral differential thrust. In addition, variations in thrust change the slipstream intensity, which further affects the control effectiveness of the aerodynamic control surfaces. Therefore, the aircraft is a typical redundant over-actuated system.

For the distributed-propulsion tandem-wing UAV studied in this paper, the front wing is located below the rear wing, and the elevons are arranged along the trailing edge of the rear wing. When longitudinal differential thrust is applied in the distributed heterogeneous electric propulsion system, variations in the rear-wing propulsion units not only generate a direct pitching moment through the vertical moment arm, but also change the local slipstream velocity and dynamic pressure over the rear wing, thereby further modifying the control effectiveness of the elevons. The combined pitching control moment generated by the aerodynamic control surfaces and differential thrust is therefore not a simple linear superposition of the two effects. Instead, the slipstream velocity downstream of each rear-wing propulsion unit must be calculated according to its actual thrust, and the control effectiveness of the aerodynamic surfaces under slipstream effects should then be evaluated and superimposed in real time. For clarity in the following analysis, the distributed heterogeneous propulsion units are numbered from 1 to 8, in the order from the front wing to the rear wing and from left to right. The elevon segmentation under slipstream effects is shown in Figure 11.

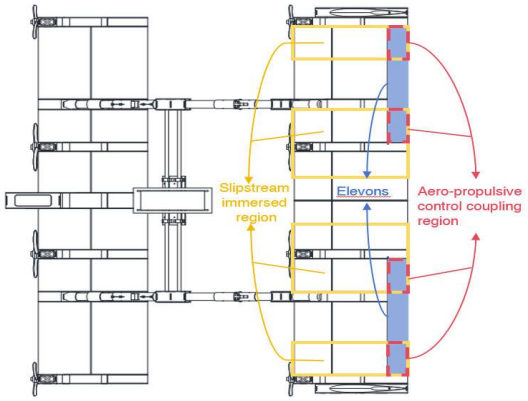


Figure 11 – Segmentation of the rear-wing elevons under slipstream effects.

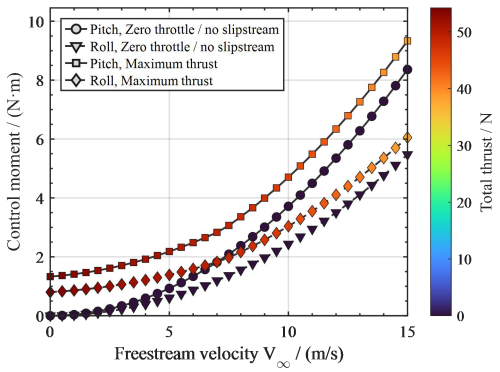


Figure 12 – Maximum control moments of the elevons under different thrust conditions.

To describe this coupling relationship, the elevons are first divided into different regions according to their relative positions with respect to the propeller slipstreams. Specifically, the elevon area is divided into the outboard-propeller slipstream-affected region, the freestream region, and the inboard-propeller slipstream-affected region. Based on the area of each region and its relative position with respect to the center of gravity, the pitching and rolling control effectiveness of each elevon region is recalculated. The calculated results are listed in Table 1.

Table 1 – Control effectiveness coefficients of the segmented elevons

Region	Control mode	Control effectiveness
Outboard-propeller slipstream-affected region	Pitch	-0.090
	Roll	-0.0201
Freestream region	Pitch	-0.141
	Roll	-0.0234
Inboard-propeller slipstream-affected region	Pitch	-0.101
	Roll	-0.0104

Since the adopted control effectiveness coefficients are nondimensional coefficients for a single control surface, a factor of 2 should be applied when the control surfaces on both sides act simultaneously. Therefore, the rolling moment generated by the elevons under the influence of propeller slipstreams can be expressed as follows:

$$L_{\delta a,\mathrm{slip}} = 2Sb\delta_a\left(2C_{l\delta a,\mathrm{free}}q_{\mathrm{free}} + C_{l\delta a,\mathrm{os}}q_{\mathrm{slip},5} + C_{l\delta a,\mathrm{is}}q_{\mathrm{slip},6} + C_{l\delta a,\mathrm{is}}q_{\mathrm{slip},7} + C_{l\delta a,\mathrm{os}}q_{\mathrm{slip},8}\right) \tag{10}$$

where q_{free} is the freestream dynamic pressure, and $q_{\mathrm{slip},i}$ denotes the corrected equivalent dynamic pressure of the propeller slipstream generated by each rear-wing propulsion unit. $C_{l\delta a,\mathrm{free}}$, $C_{l\delta a,\mathrm{os}}$, and $C_{l\delta a,\mathrm{is}}$ are the rolling control effectiveness derivatives of the elevons in the freestream region, the outboard-propeller slipstream region, and the inboard-propeller slipstream region, respectively.

Similarly, the pitching moment generated by the elevons under the influence of propeller slipstreams can be expressed as follows:

$$M_{\delta e,\mathrm{slip}} = 2Sc\delta_e\left(2C_{m\delta e,\mathrm{free}}q_{\mathrm{free}} + C_{m\delta e,\mathrm{os}}q_{\mathrm{slip},5} + C_{m\delta e,\mathrm{is}}q_{\mathrm{slip},6} + C_{m\delta e,\mathrm{is}}q_{\mathrm{slip},7} + C_{m\delta e,\mathrm{os}}q_{\mathrm{slip},8}\right) \tag{11}$$

Where $C_{m\delta e,\mathrm{free}}$, $C_{m\delta e,\mathrm{os}}$, and $C_{m\delta e,\mathrm{is}}$ denote the pitching control effectiveness derivatives of the elevons in the freestream region, the outboard-propeller slipstream region, and the inboard-propeller slipstream region, respectively.

In addition to generating total thrust, the distributed propulsion system can also produce control moments through longitudinal and lateral differential thrust. The pitching moment generated by differential thrust in the distributed propulsion system can be expressed as follows:

$$M_{\text{thrust}} = h_f \sum_{i=1}^{4} T_i - h_r \sum_{i=5}^{8} T_i \tag{12}$$

where h_{f} and h_{r} denote the vertical distances from the front-wing propulsion units and rear-wing propulsion units to the center of gravity, respectively. Similarly, the yawing moment generated by differential thrust can be expressed as follows:

$$N_{\text{thrust}} = l_o\left(T_1 + T_5 - T_4 - T_8\right) + l_i\left(T_2 + T_6 - T_3 - T_7\right) \tag{13}$$

where l_{o} and l_{i} denote the lateral moment arms of the outboard and inboard propulsion units with respect to the center of gravity, respectively. In this paper, the additional rolling moment contribution caused by the asymmetric slipstream distribution induced by lateral differential thrust is not considered.

Since the elevon effectiveness depends on the rear-wing thrust, the pitching moment jointly generated by the elevons and differential thrust should be expressed as the sum of the direct pitching moment produced by differential thrust and the elevon pitching moment under the current rear-wing slipstream conditions:

$$M_{\text{total}} = M_{\delta e,\text{slip}} + M_{\text{thrust}} \tag{14}$$

To further analyze the influence of propeller slipstreams on the control capability of the elevons, the pitching and rolling moments generated by the elevons at their maximum deflection are calculated under two representative propulsion conditions, namely zero thrust and maximum thrust, based on the slipstream correction model and the control effectiveness model described above. The calculated results are shown in Figure 12, where the color of each marker represents the total thrust of the aircraft under the corresponding condition.

As shown in the figure, under the maximum control-surface deflection, both the pitching moment and the rolling moment generated by the elevons increase with freestream velocity. Under the zero-thrust condition, the control moment produced by the control surfaces is mainly determined by the freestream dynamic pressure; therefore, the control capability is relatively weak in the low-speed range. Under the maximum-thrust condition, the propeller slipstreams increase the local dynamic pressure over the control-surface region, enabling the elevons to generate certain control moments even at low or near-zero freestream velocities. As the freestream velocity increases, the freestream dynamic pressure gradually becomes dominant, and the relative contribution of slipstream-induced augmentation decreases. Nevertheless, the control moments under the maximum-thrust condition remain generally higher than those under the zero-throttle condition. These results indicate that propeller slipstreams can effectively enhance the pitching and rolling control capability of the elevons during the low-speed takeoff phase.

3.2 Attainable Set of Coupled Pitching Moment from Differential Thrust and Elevons under Slipstream Effects

During the fixed-point high-pitch takeoff to steady climb phase, control allocation must not only satisfy the required moment commands, but also ensure sufficient vertical load-carrying capability and forward acceleration capability. To guarantee safety during liftoff and climb, the vertical load factor and horizontal load factor are introduced as feasibility constraints on the thrust combinations. In addition, to avoid distortion of the control margin caused by rapid variations in aerodynamic coefficients after stall, the attainable-set search is restricted to angles of attack below the stall angle. The constraints used for the attainable-set calculation are listed in Table 2.

Table 2 – Constraints for pitching moment attainable set calculation

Parameter	Constraint
V_{free}	$0\ \text{m/s} \le V_{\text{free}} \le 15\ \text{m/s}$
α	$\alpha \le \alpha_{\text{stall}}$
δ_e	$-25° \le \delta_e \le 25°$
n_z	$0.2 \le n_z$
n_x	$0.2 \le n_x$
$\delta_{t,i}$	$0 \le \delta_{t,i} \le 1$

Based on the propeller slipstream correction model and the control effectiveness model established above, the pitching moment attainable sets are calculated for three cases: elevons acting alone, differential thrust acting alone, and the combined effect considering the coupling between the rear-wing slipstream and the elevons. In the calculation of the combined attainable set, the thrust limits, angle-of-attack constraint, vertical load factor constraint, and minimum horizontal load factor constraint are all taken into account. Therefore, the obtained results reflect not only the limiting control capability of the effectors themselves, but also the restrictions imposed on the available pitching moment by flight safety requirements during fixed-point high-pitch takeoff and climb. The pitching moment attainable set obtained when both the inboard and outboard propulsion units participate in differential thrust is shown in Figure 13.

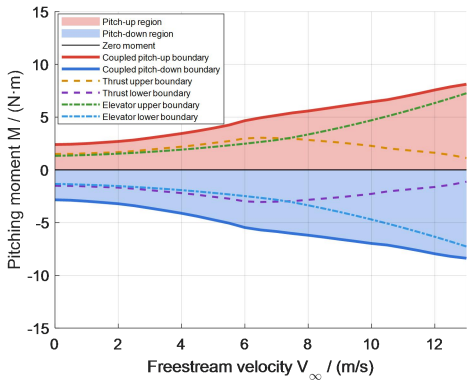


Figure 13 –Coupled pitching moment attainable set with both inboard and outboard differential thrust

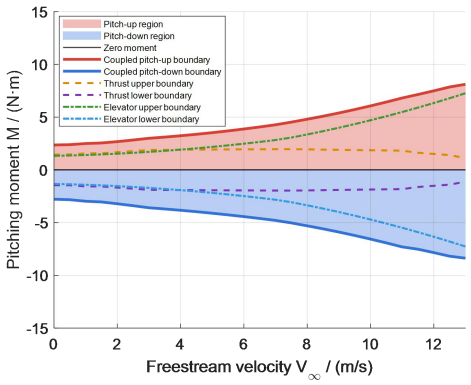


Figure 14 –Coupled pitching moment attainable set with outboard differential thrust only

The calculation results show that, under the given thrust capability and takeoff safety constraints, the maximum pitch-up and pitch-down moments generated by the combined action of elevons and differential thrust are generally asymmetric. This is because longitudinal differential thrust not only produces a direct pitching moment through the thrust moment arm, but also changes the slipstream intensity over the rear wing, thereby affecting the pitching effectiveness of the elevons immersed in the slipstream. Therefore, the coupled pitching moment boundary is not a simple linear superposition of the elevon and differential-thrust moment boundaries, but is jointly determined by thrust allocation, slipstream augmentation, control-surface effectiveness, and safety constraints. In the low-speed range, the propeller slipstream significantly increases the local dynamic pressure over the rear-wing elevons, allowing them to provide effective pitching control moments. Although differential thrust can also generate pitching moments directly, its available margin is limited because the thrust must simultaneously satisfy vertical load-carrying and forward acceleration requirements during takeoff and climb. Therefore, differential thrust is not significantly superior to the aerodynamic control surfaces at low speeds, and using both effectors is more beneficial for expanding the attainable moment range and improving the control margin during the initial takeoff phase.

A further comparison between the two schemes, namely differential thrust using both inboard and outboard propulsion units and differential thrust using only the outboard propulsion units, shows that the former can provide slightly larger differential-thrust pitching moments in part of the low-to-medium speed range. However, its contribution to expanding the coupled pitching moment attainable set is not significant. In addition, when both inboard and outboard propulsion units participate in differential thrust, thrust variations have a stronger coupled influence on slipstream-induced lift and drag as well as elevon effectiveness, leading to more pronounced nonsmooth variations in the attainable set boundary. In contrast, when only the outboard propulsion units participate in pitching differential thrust, the inboard propulsion units can remain symmetric to provide baseline thrust and stable slipstream augmentation, while the outboard propulsion units mainly undertake the pitching differential control task. This results in a smoother boundary of the coupled attainable set. Therefore, considering control capability, control allocation complexity, and engineering practicality, this paper adopts the scheme in which only the outboard propulsion units participate in pitching differential thrust.

3.3 Control Allocation Design Based on the Pitching Moment Attainable Set

The pitch channel of the aircraft studied in this paper is jointly affected by the rear-wing elevons and longitudinal differential thrust, and a coupling relationship exists between them due to propeller slipstream effects. Therefore, this paper focuses on the control allocation design for the pitch channel.

According to the attainable-set analysis presented above, both differential thrust and slipstream-augmented elevons can provide a certain level of pitching control capability during the low-speed takeoff phase. However, their control effectiveness varies rapidly with airspeed, angle of attack, and thrust state. Considering that this low-speed phase lasts for only a short period, the use of a complex real-time optimization-based allocation method would not only require highly accurate online estimation of control effectiveness, but could also introduce abrupt allocation changes and increase engineering implementation complexity. Therefore, a parallel control strategy is adopted in the low-speed phase: the pitch control command is simultaneously applied to the elevons and differential thrust, allowing both effectors to jointly generate the required pitching control moment and improve the control margin during the initial takeoff phase.

As the flight speed increases, the dynamic pressure over the elevon region increases, thereby enhancing the pitching control capability of the elevons. At the same time, the thrust margin available for pitch differential control gradually decreases, reducing the benefit of continuing to use differential thrust. Based on this consideration, a speed-scheduled control allocation strategy is adopted. In the low-speed range, both the elevons and differential thrust participate in pitch control. Within the transition speed range, the weighting factor of differential thrust decreases gradually with increasing airspeed. Once the airspeed exceeds the prescribed upper threshold, differential thrust is removed from the pitch channel, and pitch control is mainly provided by the elevons. This strategy preserves the additional control authority available at low speeds while reducing unnecessary propulsion-system regulation at higher speeds. Based on the above analysis, the following piecewise scheduling strategy is adopted in this paper:

$$\begin{cases} \delta_e = k_e u_m, \quad \delta_{dt} = k_T u_m, & V_{\text{free}} < V_1 \\ \delta_e = k_e u_m, \quad \delta_{dt} = \lambda_T k_T u_m, & V_1 \le V_{\text{free}} < V_2 \\ \delta_e = k_e u_m, \quad \delta_{dt} = 0, & V_{\text{free}} \ge V_2 \end{cases} \tag{15}$$

where u_m denotes the virtual pitching moment command, δ_e is the elevon deflection command, and $\delta_{\text{dt}}$is the differential-thrust command. k_e and k_T are the proportional gains for elevon control and differential-thrust control, respectively. Based on the pitching moment attainable set obtained with the combined use of elevons and differential thrust, $V_1 = 6\ m/s$ and $V_2 = 8\ m/s$ are selected. The differential-thrust weighting function is defined as follows:

$$\lambda_T = \frac{V_2 - V_{\text{free}}}{V_2 - V_1}, \quad V_1 \le V_{\text{free}} < V_2 \tag{16}$$

This strategy avoids complex real-time allocation during the rapidly varying low-speed phase. Meanwhile, the transition speed range reduces abrupt control changes caused by effector switching, while preserving the control benefits provided by the coupling between distributed propulsion and aerodynamic control surfaces. Therefore, the proposed strategy has good engineering feasibility.

4. Fixed-Point High-Angle-of-Attack Takeoff Simulation Verification of the Control Allocation Strategy under Slipstream Effects

4.1 Attitude Control Loop for Fixed-Point High-Angle-of-Attack Takeoff

To verify the attitude control capability of the proposed distributed-propulsion tandem-wing UAV during fixed-point high-angle-of-attack takeoff, closed-loop simulations are further conducted for the process from fixed-point high-angle-of-attack takeoff to steady climb. During the initial stage of fixed-point high-angle-of-attack takeoff, the flight speed is low, the attitude changes rapidly, and the aircraft has not yet entered a stable trajectory-tracking phase. If an outer-loop position controller is directly introduced at this stage, it may lead to position-error integration, abrupt velocity commands,

and excessive attitude commands, which are unfavorable for takeoff safety analysis. Therefore, an outer-loop position control loop is not adopted in this phase. Instead, an attitude inner-loop control approach is used, allowing the aircraft to prioritize attitude establishment and steady climb.

The attitude control loop adopts an angle–angular rate cascaded PI control structure. The outer loop is the attitude-angle control loop, which generates angular rate commands based on the error between the desired attitude angles and the current attitude angles. The inner loop is the angular-rate control loop, which generates the corresponding control commands according to the error between the commanded and actual angular rates. This cascaded structure improves attitude response speed and angular-rate damping while maintaining a simple control-law form, making it suitable for the strongly coupled, low-speed flight conditions with significant slipstream effects during the initial takeoff phase.

In the simulation, the pitch angle command is set to $45°$ to represent the target attitude for the transition from fixed-point takeoff to steep climb. The roll and yaw angle commands are both set to $0°$, so as to maintain lateral attitude stability and avoid heading deviation. Therefore, the attitude command can be expressed as follows:

$$\theta_c = 45^\circ, \quad \phi_c = 0^\circ, \quad \psi_c = 0^\circ \tag{17}$$

where θ_c, ϕ_c and ψ_c denote the pitch angle command, roll angle command, and yaw angle command, respectively.

4.2 Comparative Simulation Setup for Control Allocation Design Verification

To further verify the effectiveness and necessity of the proposed control allocation strategy during fixed-point high-angle-of-attack takeoff, four control schemes are designed for comparative simulations. Scheme A is a fixed-speed-threshold switching scheme. When the airspeed is below 6 m/s, only differential thrust is used for pitch control; when the airspeed is greater than or equal to 6 m/s, differential thrust is gradually removed, and pitch control is mainly undertaken by the elevons. Scheme B uses the elevons and differential thrust simultaneously over the entire speed range, and is used to examine the effect of continuous differential-thrust participation without speed scheduling. Scheme C is the speed-scheduled control allocation strategy proposed in this paper based on the pitching moment attainable set. In this scheme, the elevons and differential thrust jointly participate in pitch control in the low-speed range, while differential thrust is gradually removed from the pitch channel as the airspeed increases. Scheme D is the no-slipstream aerodynamic model scheme, in which the enhancement of the local dynamic pressure over the wing and elevons caused by propeller slipstreams is not considered in the dynamic model. By comparing the attitude response, speed build-up process, control-surface deflection, differential-thrust command, and thrust variation among the four schemes, the improvements achieved by the proposed method can be comprehensively evaluated in terms of low-speed control margin, rational use of effectors, and stability during takeoff and climb.

4.3 Simulation Results and Analysis of the Control Allocation Strategy under Slipstream Effects

To verify the effectiveness of the pitching moment attainable set-based speed-scheduled control allocation strategy during fixed-point high-angle-of-attack takeoff, closed-loop comparative simulations of the four control schemes were conducted under the same initial conditions and control parameters.

As shown in Figure 15, all four schemes can make the pitch angle converge to approximately 45◦ in the later stage, indicating that the attitude inner loop can accomplish the attitude-holding task during the transition from fixed-point high-angle-of-attack takeoff to steady climb. However, noticeable differences exist in their transient responses. In Scheme A, pitch control relies only on differential thrust in the low-speed range, resulting in a relatively large pitch-angle overshoot and pitch-rate peak during the initial takeoff phase. In contrast, Schemes B and C both employ the elevons and differential thrust for pitch control at low speeds, which effectively reduces the overshoot and pitch-rate peak. This indicates that the combined use of aerodynamic control surfaces and differential thrust improves the smoothness of the attitude response during the initial takeoff phase. The attitude response of Scheme C is close to that of Scheme B, demonstrating that

the proposed speed-scheduled control allocation strategy can maintain good attitude-tracking performance while reducing the continuous use of differential thrust.

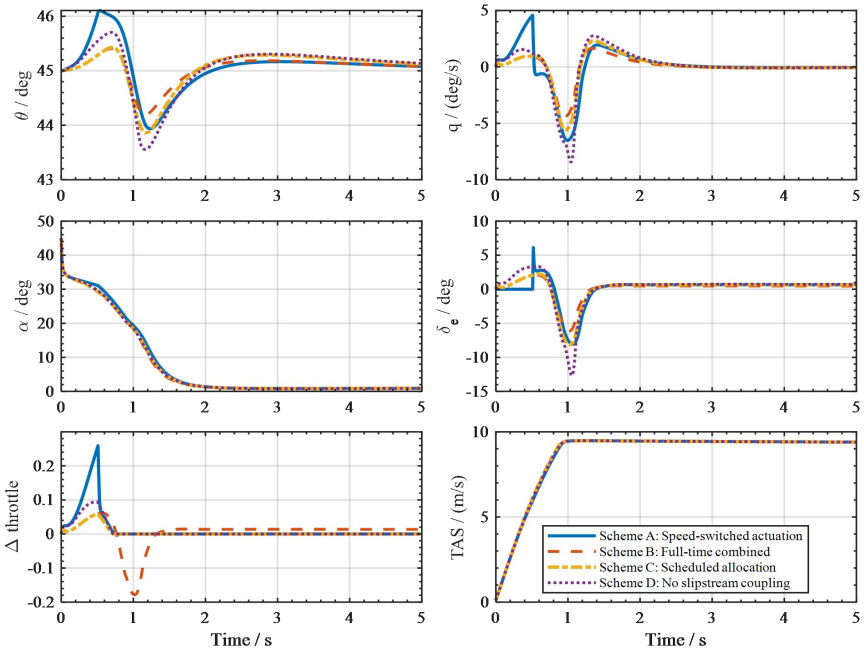


Figure 15 – Closed-loop response comparison of different control allocation schemes during fixed-point high-angle-of-attack takeoff

From the perspective of effector usage, Scheme A generates a relatively large differential-throttle command in the low-speed range and rapidly removes differential thrust after reaching the switching speed. This indicates that fixed-threshold switching causes the propulsion system to undertake strong attitude regulation during the initial takeoff phase and may introduce response fluctuations near the switching point. Scheme B improves the attitude response, but it continuously uses differential thrust over the entire speed range. According to the attainable-set analysis above, as the airspeed increases, the control capability of the elevons increases, whereas the available margin for differential thrust decreases. Therefore, continuing to use differential thrust at higher speeds provides limited benefit and increases the regulation burden on the propulsion system. In contrast, Scheme C uses differential thrust only to supplement the pitching moment in the low-speed range, with a smaller differential-throttle command that quickly approaches zero, indicating a more rational allocation of control effort among the effectors.

Scheme D does not include the enhancement of the local dynamic pressure over the wing and elevons caused by propeller slipstreams in the dynamic model. Therefore, the low-speed control capability of the elevons is mainly limited by the freestream dynamic pressure. The simulation results show that Scheme D requires larger elevon deflections during the initial takeoff phase and exhibits more pronounced pitch-rate fluctuations. This confirms that propeller slipstreams significantly enhance the control capability of aerodynamic control surfaces at low speeds and should be considered in dynamic modeling and control allocation simulations.

Overall, Scheme C achieves an attitude response close to that of the full-time combined control in Scheme B, while significantly reducing the continuous use of differential thrust. Compared with Scheme A, Scheme C avoids the large attitude overshoot and differential-throttle peak caused by relying solely on differential thrust at low speeds. Compared with Scheme D, Scheme C reflects the improvement in low-speed elevon effectiveness provided by slipstream augmentation. Therefore, the pitching moment attainable set-based speed-scheduled control allocation strategy proposed in this paper can maintain attitude-tracking performance while reducing differential-thrust usage and control-surface deflection peaks, thereby balancing low-speed control margin, rational effector usage, and smoothness during takeoff and climb.

5. Conclusions

This paper investigates propeller slipstream modeling, attainable moment set calculation of coupled effectors, and pitch-channel control allocation for a distributed heterogeneous electric propulsion tandem-wing UAV adopting a fixed-point high-pitch-angle takeoff mode.

- A propeller slipstream model considering slipstream contraction, slipstream-affected area, and finite-height correction is established. A velocity-ratio saturation mechanism is introduced to avoid model singularity under zero-freestream conditions. Ground static test results show that the predicted slipstream velocity and slipstream-induced lift agree well with the experimental measurements, validating the effectiveness of the proposed model.
- Considering that the rear-wing elevons are directly affected by the propeller slipstream, the influence of slipstream-induced augmentation on control-surface effectiveness is analyzed. The pitching moment attainable sets of the elevons, differential thrust, and their coupled action are then calculated. The results show that, under thrust limits, angle-of-attack constraints, and load-factor constraints, the coupled pitching moment boundary exhibits asymmetric characteristics. Considering control capability, boundary smoothness of the attainable set, and engineering feasibility, the scheme in which only the outboard propulsion units participate in pitching differential thrust is adopted.
- Based on the attainable moment set analysis, a speed-scheduled control allocation strategy is proposed. In the low-speed range, the elevons and differential thrust jointly participate in pitch control; in the transition range, the differential-thrust weighting factor gradually decreases; and at higher speeds, pitch control is undertaken solely by the elevons. Closed-loop simulation results show that the proposed strategy reduces the use of differential thrust and the peak elevon deflection while maintaining pitch-angle tracking performance, and further demonstrates the important role of slipstream-induced augmentation in improving the low-speed control capability of aerodynamic surfaces.

6. Contact Author Email Address

Yuhang Xie: yuhangxie@mail.nwpu.edu.cn

7. Copyright Statement

The authors confirm that they, and/or their company or organization, hold copyright on all of the original material included in this paper. The authors also confirm that they have obtained permission, from the copyright holder of any third party material included in this paper, to publish it as part of their paper. The authors confirm that they give permission, or have obtained permission from the copyright holder of this paper, for the publication and distribution of this paper as part of the ICAS proceedings or as individual off-prints from the proceedings.

References

[1] Huang J. Survey on design technology of distributed electric propulsion aircraft. *Acta Aeronautica et Astronautica Sinica*, Vol. 42, No. 3, Article 624037, 2021.

[2] Borer N K, Patterson M D, Viken J K, Moore M D, Clarke S, Redifer M E, Christie R J, Stoll A M, Dubois A, Bevirt J, Gibson A R, Foster T J and Osterkamp P G. Design and performance of the NASA SCEPTOR distributed electric propulsion flight demonstrator. *Proc 16th AIAA Aviation Technology, Integration, and Operations Conference*, Washington, D.C., AIAA 2016-3920, 2016.

[3] Kim H D, Perry A T and Ansell P J. A review of distributed electric propulsion concepts for air vehicle technology. *Proc 2018 AIAA/IEEE Electric Aircraft Technologies Symposium,* Cincinnati, Ohio, *AIAA* 2018-4998, pp 1-21, 2018.

[4] Pieper K, Perry A, Ansell P and Bretl T. Design and development of a dynamically scaled distributed electric propulsion aircraft testbed. *Proc 2018 AIAA/IEEE Electric Aircraft Technologies Symposium,* Cincinnati, Ohio, AIAA 2018-4996, 2018.

[5] Rothhaar P M, Murphy P C, Bacon B J, Gregory I M, Grauer J A, Busan R C and Croom M A. NASA Langley distributed propulsion VTOL tilt-wing aircraft testing, modeling, simulation, control, and flight test development. *Proc 14th AIAA Aviation Technology, Integration, and Operations Conference,* Atlanta, Georgia, AIAA 2014-2999, 2014.

[6] Ting L, Liu C H and Kleinstein G. Interference of wing and multipropellers. *AIAA Journal*, Vol. 10, No. 7, pp 906-914, 1972.

[7] Nederlof R. Improved modeling of propeller-wing interactions with a lifting-line approach. MSc Thesis, Delft University of Technology, 2020.

[8] Qin J, Zhou Z, Yang G, et al. Aero-propulsive coupling modeling and dynamic stability analysis of distributed electric propulsion tandem-wing UAV with rapid ascent capability. *Aerospace Science and Technology*, Vol. 153, pp 109406, 2024.
[9] Patterson M D, Derlaga J M and Borer N K. High-lift propeller system configuration selection for NASA's SCEPTOR distributed electric propulsion flight demonstrator. *16th AIAA Aviation Technology, Integration, and Operations Conference*, 2016.
[10] Qin Z, Wei J and Liu K. A uniform control allocation method for distributed electric propulsion aircraft using iterative-based approach and coordinate transformation. *Proc 2023 42nd Chinese Control Conference*, Tianjin, China, pp 3079-3085, 2023.
[11] Wang Z, Zhang J and Yang L. Weighted pseudo-inverse based control allocation of heterogeneous redundant operating mechanisms for distributed propulsion configuration. *Energy Procedia*, Vol. 158, pp 1718-1723, 2019.
[12] Suiçmez E C and Kutay A T. Full envelope nonlinear flight controller design for a novel electric VTOL air taxi. *The Aeronautical Journal*, Vol. 128, pp 966-993, 2024.
[13] de Heer P, de Visser C C, Hoogendoorn M L and Jentink H W. Incremental nonlinear control allocation for an aircraft with distributed electric propulsion. *Proc AIAA SCITECH 2023 Forum*, National Harbor, Maryland and Online, AIAA 2023-1248, 2023.
[14] Yılmaz E and German B J. Control allocation optimization for an over-actuated tandem tiltwing eVTOL aircraft considering aerodynamic interactions. *Aerospace Science and Technology*, Vol. 155, Article 109595, 2024.
[15] McCormick B W. Aerodynamics of V/STOL flight. *Courier Corporation*, 1999.